ARTICLES
PUBLISHED ONLINE: 30 JANUARY 2011 | DOI: 10.1038/NPHYS1903
nature physics

Observations and simulations of non-local acceleration of electrons in magnetotail magnetic reconnection events

Maha Ashour-Abdalla[1]*, Mostafa El-Alaoui[1], Melvyn L. Goldstein[2], Meng Zhou[3], David Schriver[1], Robert Richard[1], Raymond Walker[1], Margaret G. Kivelson[1,4] and Kyoung-Joo Hwang[2,5]

Magnetic reconnection in magnetized plasmas represents a change in magnetic field topology and is associated with a concomitant energization of charged particles that results from a conversion of magnetic energy into particle energy. In Earth's magnetosphere this process is associated with the entry of the solar wind into the magnetosphere and with the initiation of auroral substorms. Using data from the THEMIS mission, together with global and test particle simulations, we demonstrate that electrons are energized in two distinct regions: a low-energy population (less than or equal to a few kiloelectronvolts) that arises in a diffusion region where particles are demagnetized and the magnetic topology changes, and a high-energy component (approaching 100 keV) that results from betatron acceleration within dipolarization fronts that sweep towards the inner magnetosphere far from the diffusion region. Thus, the observed particle energization is associated with both magnetic reconnection and with betatron acceleration associated with macroscopic flows.

We propose a solution to the problem of where and how electrons are accelerated in the magnetotail during periods of substorm activity[1]. Substorms are commonly thought to be a consequence of the reconnection of magnetic fields in the tail, which occurs in narrow current sheets bounded by oppositely directed magnetic fields. The conversion of magnetic energy into particle energy associated with reconnection will occur naturally near the electron and ion diffusion regions where the particles are demagnetized. However, what has not been clear is whether all energetic particles are accelerated in the vicinity of the diffusion regions. Several early studies have discussed how induced electric fields can accelerate particles[2–4]. Åsnes *et al.*[5] have recently described the general circumstances surrounding energization in reconnection.

Recent observations in Earth's magnetotail have shown rapid increases in electron fluxes, with energies up to hundreds of kiloelectronvolts, that are associated with earthward-moving dipolarization fronts[6,7] (K-J.H. *et al.* manuscript in preparation) penetrating into the inner magnetosphere. Moreover, the electron population within a dipolarization front responds differently at high and low energies. The fluxes increase at high energies and tend to decrease at lower energies[8–10] (K-J.H. *et al.* manuscript in preparation). The observations seem to indicate that at least two processes are occurring: acceleration near the site of reconnection[11–15] and a global process related to the magnetic field reconfiguration that operates as the flow moves from the reconnection site to the inner magnetosphere and the magnetic field becomes more dipolar[7,16,17]. The non-Maxwellian distributions that ensue are unstable to the generation of waves, including large-amplitude electric field emissions in the lower hybrid frequency range, emissions in the whistler frequency range and emissions above the electron cyclotron frequency[18] (K-J.H. *et al.* manuscript in preparation).

Several theoretical efforts to understand electron acceleration in the magnetotail have focused on local acceleration processes at the reconnection points. Processes considered include acceleration by the reconnection electric field or stochastic processes associated with turbulent structures near the reconnection X-line[19–26]. However, by their nature, such studies cannot address the possibility that considerable acceleration may occur away from the neutral line. Investigation of that option requires a more global analysis. In this article, we argue that the use of both kinetic and global simulations can answer the question of where and how electrons are accelerated in the magnetotail during substorm-driven dipolarization events. The approach uses Vlasov–Maxwell theory together with the construction of particle distribution functions from THEMIS plasma data to locate where in the magnetotail and by what process a non-local population of electrons is energized.

Processes that might accelerate electrons far from the diffusion regions have been proposed from at least the late 1970s. They include betatron acceleration[2,3], also recently invoked to explain electron acceleration signatures observed in the magnetotail in association with substorms[7]. In addition, Hoshino[27] and Imada[16] invoked non-adiabatic motion in magnetospheric electric and magnetic fields, which can occur as the dipolarization of the magnetic field moves from the mid- or distant tail earthward.

In this article, we describe observations of fields and particles obtained during a substorm, using data from the THEMIS satellites. We then employ both global and large-scale-kinetic (LSK) simulations to trace where and how electrons are accelerated.

[1]Institute for Geophysics and Planetary Physics, University of California, Los Angeles, Los Angeles, California 90095-1567, USA, [2]NASA Goddard Space Flight Center, Code 673, Greenbelt, Maryland 20771, USA, [3]Institute of Space Science and Technology, Nanchang University, 330031, China, [4]Department of Atmospheric, Oceanic and Space Sciences, University of Michigan, Ann Arbor, Michigan 48109, USA, [5]University of Maryland, Baltimore County, Maryland 21250, USA. *e-mail: mabdalla@igpp.ucla.edu.

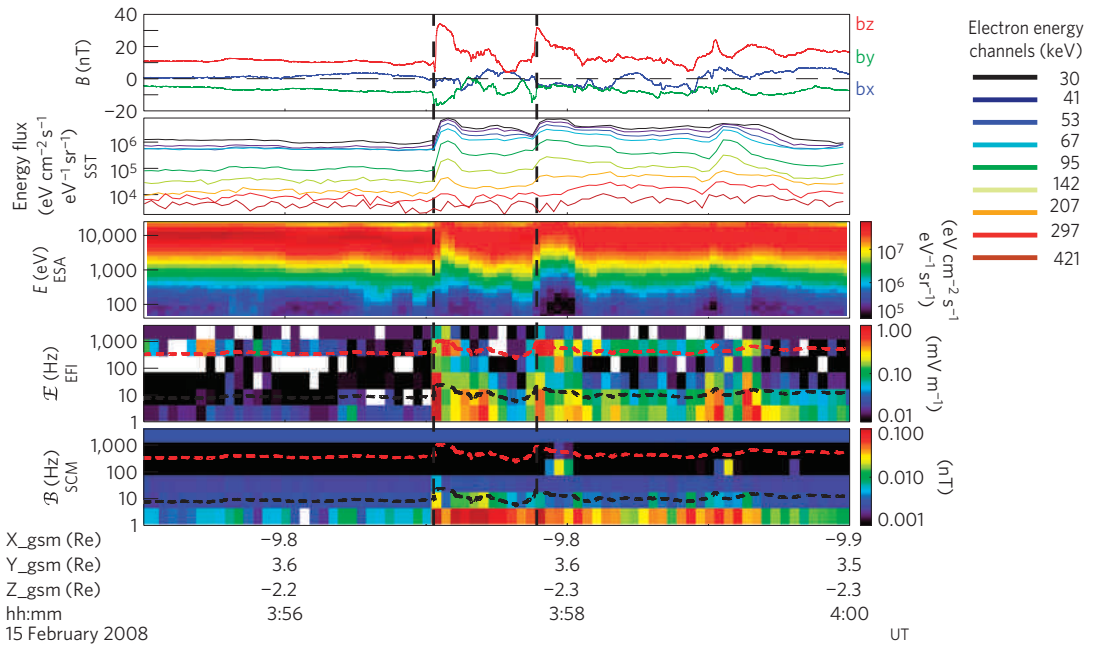

Figure 1 | Observations from THEMIS P4 on 15 February 2008. The three curves in the top panel contain the three components of the magnetic field in GSM coordinates. The second panel gives energy fluxes of energetic electrons from the SST instrument with the energy scale on the right. A spectrogram of the energy flux from the ESA instrument is shown in the third panel. Dynamic spectra of the electric and magnetic field waves are shown in the last two panels. The dashed lines give the lower hybrid (black) and electron cyclotron frequencies (red).

Finally we compare our simulation results with THEMIS data to argue that electron acceleration occurs both at the reconnection region and at dipolarization fronts as a result of the betatron effect.

Observations

On 15 February 2008 there was a large substorm during which time three of the THEMIS satellites were grouped in the near-Earth tail between $x \approx -12\,R_E$ and $x = -8\,R_E$ (in Geocentric Solar Magnetospheric coordinates (GSM)). They were near the equator and $y \sim 2\,R_E$ duskward of midnight[18]. In addition to the d.c. magnetic field and both thermal and energetic particle data, the THEMIS spacecraft provided burst-mode (high temporal resolution) plasma wave observations. Data acquired by the THEMIS P4 spacecraft are plotted in Fig. 1. The top panel shows the three components of the magnetic field[28]. The energy fluxes of energetic electrons observed by the solid-state telescope[29] (SST) instrument are plotted in the second panel. The third panel contains spectrograms of thermal energy fluxes from the electrostatic analyser[30] (ESA). The last two panels respectively show spectrograms of the electric field wave amplitude from the electric field instrument[31] (EFI) and the magnetic field wave amplitudes from the search coil magnetometer[32] (SCM). The dashed lines on the wave plots give the lower hybrid (f_{lh}, black) and the electron cyclotron (f_{ce}, red) frequencies. During the substorm expansion phase, THEMIS P4 detected two dipolarization fronts: one at 3:57:00 UT and the second one at 3:57:38 UT. The dipolarization fronts (dashed lines) are characterized by rapid increases in the B_z component of the magnetic field and by an increased energy flux of energetic SST electrons. The energy flux for channels between 30 keV and 207 keV increases at the time of the dipolarization, whereas the flux of the lower thermal energy plasma measured by ESA (<30 keV) decreases. Fluxes in the two highest energy channels, that is, 297 keV and 427 keV, do not change, indicating that the upper limit for energization is ~200 keV. At the time of the dipolarization, the electric field wave amplitude was enhanced from below f_{lh} (the lower hybrid frequency) to above f_{ce} (the electron cyclotron frequency). The magnetic field wave amplitude increased below f_{lh}, except at 3:58 UT and 3:59:10 UT, when electromagnetic whistler waves were observed.

Simulation results

First we modelled the magnetospheric configuration using a magnetohydrodynamic (MHD) simulation of the magnetosphere driven by solar wind observations[8,33]. In particular we modelled the substorm event on 15 February 2008 using upstream solar wind conditions measured by the Cluster spacecraft. The MHD simulation results provide a picture of the global three-dimensional time-varying electric and magnetic field configuration for Earth's magnetosphere. Figure 2 shows results from the MHD simulations at two different times when dipolarization was occurring, at 3:56 UT and 3:59 UT. The colour coding in Fig. 2 shows the north–south (B_z) component of the magnetic field in the maximum pressure surface[34] in the magnetotail. Flow vectors have been superimposed in white. The locations of three THEMIS spacecraft (P3, P4 and P5) are also shown. Dipolarization fronts moving earthward can be seen in this format as increases in the B_z component (red regions). Two dipolarization fronts are apparent at 3:56 UT and 3:59 UT. The dipolarization front started near a neutral line at $x \sim -30\,R_E$ that was limited to a small region in y directly tailward of the THEMIS satellites[8]. The resulting narrow channel of earthward flow can be seen in Fig. 2. The first front was observed first by P4 and then by P5. The MHD results indicate that the front, for the most part, missed P3. The second front was observed by all three THEMIS spacecraft at 3:59 UT, first at P3, then at P4, and finally at P5.

We include electron kinetic effects in the global field configuration using the LSK technique. In LSK, a large number of electron trajectories are followed in the time-dependent electric and magnetic fields obtained from the MHD simulations[35]. Initially, electrons were launched from their source regions, which were determined by calculating trajectories from THEMIS P4 backwards in time. On the basis of the result of the backward calculation, one set of electrons was launched from the distant tail and a second

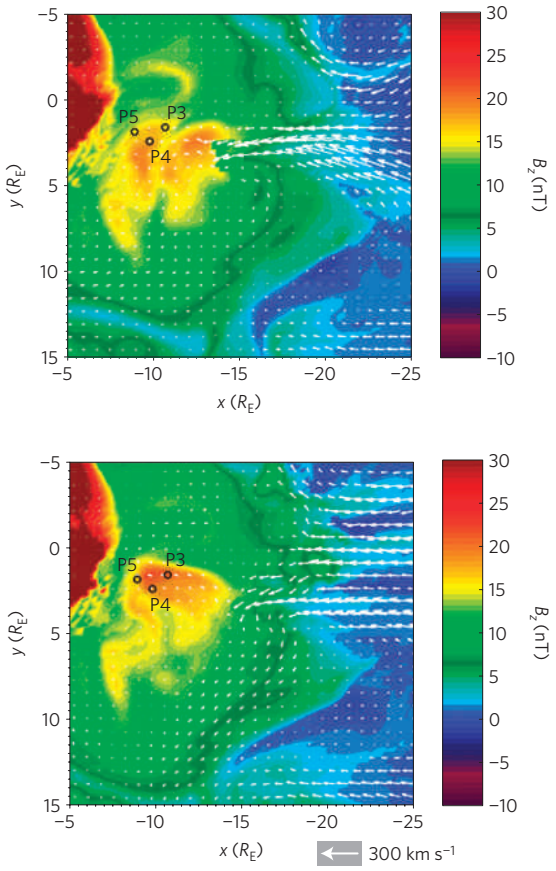

Figure 2 | B_z component of the magnetic field and flows in the maximum pressure surface. The z-component of the magnetic field (colour coded) and flow vectors (white arrows) on the maximum pressure surface from the MHD simulation for 15 February 2008. The upper panel is at 3:56 UT and the lower panel is at 3:59 UT. The locations of P3, P4 and P5 are also shown. The arrow on the bottom right corner of the plot indicates the scale of the velocity vectors.

was launched near the neutral line around $x = -20\,R_E$. These two sources are physically very reasonable. Early in the substorm the particles come from the distant tail but later in the substorm, when the near-Earth neutral line forms at about $x \sim -30\,R_E$, the source has moved earthward. The electron trajectories were followed by using a combination of full particle and guiding centre calculations[36,37]. The κ parameter, defined as the square root of the local magnetic field radius of curvature divided by the local Larmor radius[38,39], was used to determine whether full particle dynamics was necessary. When $\kappa \leq 10$, we switched from the guiding centre approximation to full particle dynamics. A large number of electrons were followed and data were collected at virtual detectors placed throughout the system[35], including the locations of the THEMIS spacecraft.

Using LSK simulations to follow electrons, we calculated the electron differential energy fluxes for various energy channels and compared these with observations at the location of THEMIS satellite P4. The results are illustrated in Fig. 3, which shows LSK calculations in the upper panel and particle data from P4 in the lower panel in terms of differential energy flux versus time in UT. The different colour curves correspond to different energy channels. For the simulation, the energies are represented as red (2–6 keV), orange (6–12 keV), green (12–25 keV), blue (25–41 keV) and black (41–95 keV). These energy bins were selected to match approximately the energy channels of the THEMIS SST and ESA detectors. It can be seen that the different energies respond differently. Specifically, starting at about 3:56 UT there are strong enhancements in the flux for the higher energies, (38.4 keV and 63.5 keV) in the observations and in the simulation (25 keV and above). In the simulation, the 12–25 keV flux (green) increases by about a factor of two. The energy flux between 6 keV and 12 keV (orange) stays approximately constant. In contrast, in the lowest energy channel (2–6 keV), the simulated energy flux decreases by about a factor of two when the dipolarization front passes. The lower energy channels in the observations also show a decrease in energy flux after dipolarization. In addition, there are two sudden decreases in energy flux between 3:57 UT and 3:58 UT. The fluxes at higher energies increase markedly at the dipolarization front. Superimposed on the overall increase there are two sharp peaks corresponding to the decreases at lower energies. The sudden decreases in the lower energy fluxes, and sharp peaks at higher energies in the observations are not seen in the simulations. There are two reasons for this. First, the changes in magnetic field (B_z) associated with the dipolarization front in the MHD simulation are more gradual than those in the observations. Second, to have a sufficient number of counts in our virtual detectors, we accumulated particles for 20 s and thereby averaged over the fine structure in the observations. In both the simulation and observations, however, there is a marked increase in the energy flux at approximately the time of the dipolarization. The conclusion from both the simulations and observations is that the energization process responsible for the increase in energy flux during the dipolarization depends on energy, and favours the higher energy particles. We have carried out similar comparisons between electrons observed at THEMIS P3 and P5. These results are included in Supplementary Discussion. Again we find reasonable agreement with observations.

To show the energization process in more detail, in Fig. 4 we have plotted the electron differential energy flux at two times (3:48 and 3:58) and in two separate energy ranges (6–12 keV and 41–95 keV) at the maximum pressure surface. At 3:48, there are few high-energy particles present anywhere. The largest fluxes of electrons in the 6–12 keV range are near the neutral line, which remained near $x \approx -19\,R_E$ at both times. At 3:58, both low-energy particles and high-energy particles are visible, and both populations are concentrated near the inner boundary of the dipolarization front (between $\approx -11\,R_E$ and $-15\,R_E$). Thus, the LSK calculations indicate that, although low-energy electrons appear immediately in the vicinity of the X-line, high-energy particles never appear near the X-line and are present only after the dipolarization front has moved inward. Low-energy particles seem to be convected with the dipolarization front and provide a seed population that is energized in the rapidly changing magnetic field of the inward-moving dipolarization front. Although there is some energization near the reconnection region, the strongest enhancements in energy flux actually occurs several R_E away from the reconnection region.

To estimate whether betatron acceleration due to the increasing magnetic field of the dipolarization can account for the electron energization in the simulation, we carried out the calculation shown in Fig. 5, where distribution functions of perpendicular energy flux versus perpendicular energy from the simulation are plotted. The calculations in Fig. 5 assume conservation of the magnetic moment, μ, which is valid under the condition that B_z changes slowly compared with the electron's gyroperiod ($\approx 10^{-3}$ s). For the event being studied, the timescale for the increase in B_z is $\approx$1–2 s, so that μ is conserved. However, it should be kept in mind that, in general, betatron acceleration will occur regardless of whether or not the time variations are such as to conserve μ.

We carried out a calculation to estimate whether betatron acceleration due to the increasing magnetic field of the dipolarization could account for the electron energization in the simulation

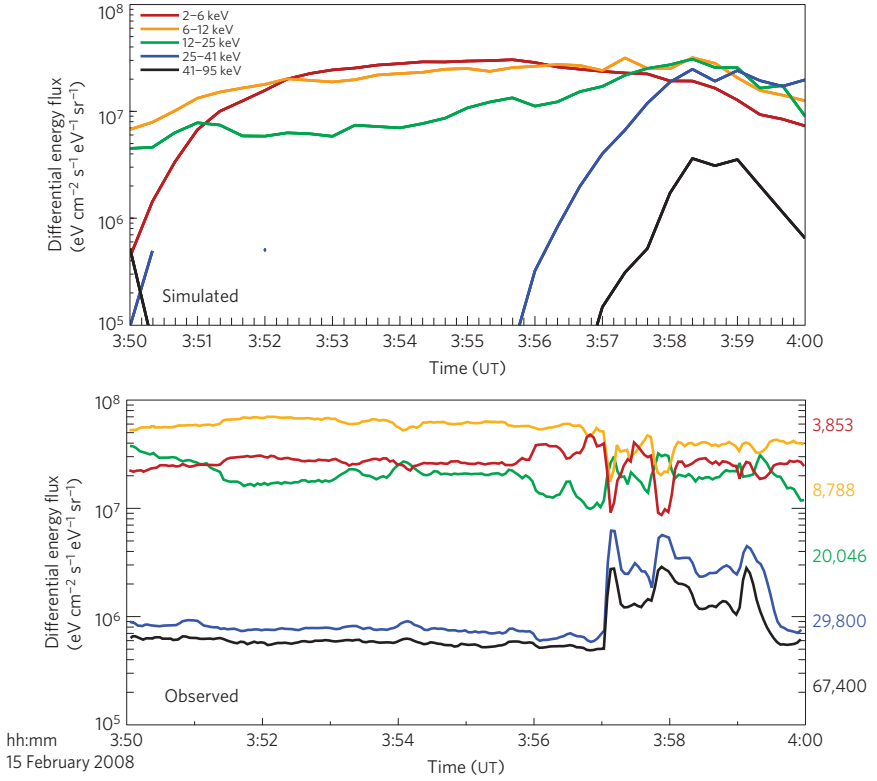

Figure 3 | Simulated energy fluxes and observed energy fluxes from THEMIS P4 observations. The energy channels for the simulation are given in the upper left corner. The energy channels for the observations are given by the scale on the right.

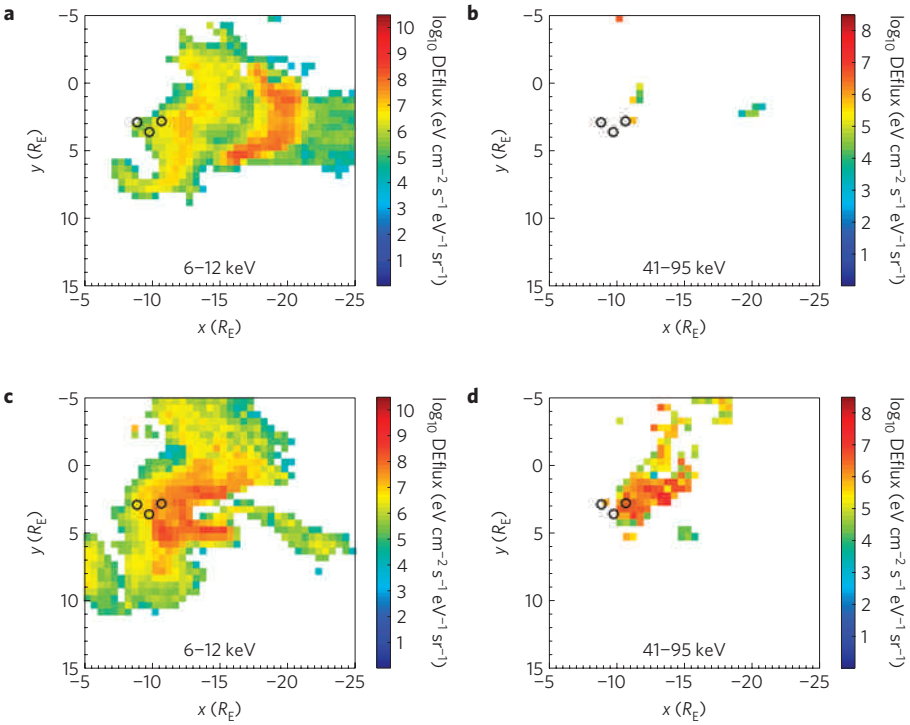

Figure 4 | Plots of differential energy flux on the maximum pressure surface for two different energy channels. a and **b** are at 3:48 UT and **c** and **d** are at 3:58 UT.

(Fig. 5). First, we determined that most of the particles observed at P4 at 3:59 UT originated in a small region ($x = \pm 1.0\,R_E, y = \pm 0.5\,R_E$) near $x = -16.8\,R_E$ and $y = 2.9\,R_E$ at approximately 3:54 UT, where an initial (perpendicular) distribution function was constructed from the simulation results in the maximum pressure plane. The average magnetic field increase in the dipolarization front was by a factor of about 2.2. The starting distribution and energy levels were then shifted by this factor and the resulting energy

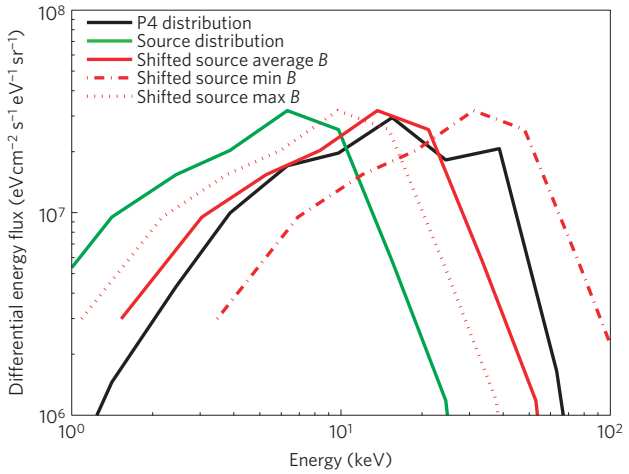

Figure 5 | Estimated change in the perpendicular energy flux from betatron acceleration in the simulation. The green curve shows the distribution of perpendicular energy flux near the source region and the solid red curve is the same distribution shifted by a factor of 2.2 in energy, based on the average magnetic field in the source region. As the magnetic field was variable in the source region, a range of shifts was possible. The minimum shift of 1.5 gives the dotted red curve and the maximum shift of 4.9 gives the chained red curve. The black curve shows the simulated distribution observed at P4. Only electrons from the X-line launches are included. Both the horizontal and vertical scales are logarithmic.

flux distribution (solid red curve) was compared to the simulated distribution at P4 (black curve). The results shown include only particles from launches near the X-line region. Considering the uncertainties in this calculation, in particular the fact that particles at a single target location can have multiple points of origin, the comparison is good. As the magnetic field in the source region was variable in space and time, we shifted the initial distribution by the maximum and minimum magnetic field ratios there to illustrate the range of betatron acceleration that was possible. These curves clearly bracket the observed distribution at P4. Other sources of uncertainty are variations in the distribution function in time and variations in the direction of **B**, which determines the division between parallel and perpendicular flux. The electrons that were launched deeper in the tail ($x = -35\,R_E$) and were observed at P4 before the arrival of the dipolarization do not experience this energization and remain at relatively low energies (not shown).

Conclusions

From the combination of the global simulations and the LSK tracing of particles, it is clear that the low energies arise near the original X-line. Higher energies are not present initially, and appear only as the dipolarization front moves earthward. The highest energies (≈ 100 keV) appear at later times in the inner magnetosphere, far from the initial X-line. Thus, the low- and high-energy electron fluxes intensify at different times and at different locales within the magnetotail.

Shock waves did not form in the magnetotail in the MHD simulation, so the acceleration observed in the LSK simulations cannot be a consequence of shock acceleration. As the location of the acceleration to the highest energies is far from the X-line, the acceleration cannot arise solely from the magnetic field gradient and curvature associated with the initial X- and O-regions[27], nor from any (local) stochastic process[19,22]. The acceleration is, however, consistent with a betatron acceleration due to the rapidly changing magnetic field, as first suggested by Kivelson in 1980 (ref. 2) and Baker *et al.* in 1982 (ref. 3).

Received 2 September 2010; accepted 3 December 2010; published online 30 January 2011

References

1. Sarris, E. T., Krimigis, S. M. & Armstrong, T. P. Observations of magnetospheric bursts of high-energy protons and electrons at approximately at 35 R_E with Imp 7. *J. Geophys. Res.* **81,** 2341–2355 (1976).
2. Kivelson, M. G. Summary remarks on the July 29, 1972 event. *EOS* **61,** 335 (1980).
3. Baker, D. N. *et al.* Observation and modelling of energetic particles at synchronous orbit on July 29, 1977. *J. Geophys. Res.* **87,** 5917–5932 (1982).
4. Sato, T., Matsumoto, H. & Nagai, K. Particle acceleration in time-developing magnetic reconnection process. *J. Geophys. Res.* **87,** 6089–6097 (1982).
5. Åsnes, A. *et al.* Multispacecraft observation of electron beam in reconnection region. *J. Geophys. Res.* **113,** A07S30 (2008).
6. Runov, A. *et al.* THEMIS observations of an earthward-propagating dipolarization front. *Geophys. Res. Lett.* **36,** L14106 (2009).
7. Asano, Y. *et al.* Electron acceleration signatures in the magnetotail associated with substorms. *J. Geophys. Res.* **115,** A05215 (2010).
8. Ashour-Abdalla, M. in *Modern Challenges in Nonlinear Plasma Physics: A Festschrift Honoring the Career of Dennis Papadopoulos* (eds Vassiliadis, D., Fung, S. F., Shao, X., Daglis, I. A. & Huba, J. D.) 196–207 (AIP Conf. Proc. 1320, American Institute of Physics, 2010).
9. Ashour-Abdalla, M., Bosqued, J. M., El-Alaoui, M., Peroomian, V. & Walker, R. Observations and simulations of a highly structured plasma sheet during northward IMF. *J. Geophys. Res.* **115,** A10227 (2010).
10. Deng, X. *et al.* Wave and particle characteristics of earthward electron injections associated with dipolarization fronts. *J. Geophys. Res.* **115,** A09225 (2010).
11. Øieroset, M., Lin, R. P., Phan, T. D., Larson, D. E. & Bale, S. D. Evidence for electron acceleration up to ~300 keV in the magnetic reconnection diffusion region of Earth's magnetotail. *Phys. Rev. Lett.* **89,** 195001 (2002).
12. Pritchett, P. L. Relativistic electron production during driven magnetic reconnection. *Geophys. Res. Lett.* **33,** L13104 (2006).
13. Pritchett, P. L. Relativistic electron production during guide field magnetic reconnection. *J. Geophys. Res.* **111,** A10212 (2006).
14. Hoshino, M. Electron surfing acceleration in magnetic reconnection. *J. Geophys. Res.* **110,** A10215 (2005).
15. Retinò, A. *et al.* Cluster observations of energetic electrons and electromagnetic fields within a reconnecting thin current sheet in the Earth's magnetotail. *J. Geophys. Res.* **113,** A12215 (2008).
16. Imada, S. *et al.* Energetic electron acceleration in the downstream reconnection outflow region. *J. Geophys. Res.* **112,** A03202 (2007).
17. Birn, J. *et al.* Substorm electron injections: Geosynchronous observations and test particle simulations. *J. Geophys. Res.* **103,** 9235–9248 (1998).
18. Zhou, M. *et al.* THEMIS observation of multiple dipolarization fronts and associated wave characteristics in the near-Earth magnetotail. *Geophys. Res. Lett.* **36,** L20107 (2009).
19. Ambrosiano, J., Matthaeus, W. & Goldstein, M. Test-particle studies of acceleration by turbulent reconnection fields. *J. Geophys. Res.* **93,** 14383–14400 (1988).
20. Hesse, M., Kuznetsova, M. & Hoshino, M. The structure of the dissipation region for component reconnection: Particle simulations. *Geophys. Res. Lett.* **29,** 1563 (2002).
21. Pritchett, P. L. & Coroniti, F. V. Three-dimensional collisionless magnetic reconnection in the presence of a guide field. *J. Geophys. Res.* **109,** A01220 (2004).
22. Drake, J. F., Swisdak, M., Che, H. & Shay, M. A. Electron acceleration from contracting magnetic islands during reconnection. *Nature* **443,** 553–556 (2006).
23. Drake, J. F. *et al.* Formation of electron holes and particle energization during magnetic reconnection. *Science* **299,** 873–877 (2003).
24. Drake, J. F., Shay, M. A., Thongthai, W. & Swisdak, M. Production of energetic electrons during magnetic reconnection. *Phys. Rev. Lett.* **94,** 095001 (2005).
25. Kowal, G., Lazarian, A., Vishniac, E. T. & Otmianowska-Mazur, K. Numerical tests of fast reconnection in weakly stochastic magnetic fields. *Astrophys. J.* **700,** 63–85 (2009).
26. Shinohara, I. *et al.* Low-frequency electromagnetic turbulence observed near the substorm onset site. *J. Geophys. Res.* **103,** 20365–20388 (1998).
27. Hoshino, M., Mukai, T., Terasawa, T. & Shinohara, I. Superthermal electron acceleration in magnetic reconnection. *J. Geophys. Res.* **106,** 25979–25978 (2001).
28. Auster, H. U. *et al.* The THEMIS fluxgate magnetometer. *Space Sci. Rev.* **141,** 235–264 (2008).
29. Angelopoulos, V. The THEMIS mission. *Space Sci. Rev.* **141,** 5–34 (2008).
30. McFadden, J. P. *et al.* THEMIS ESA first science results and performance issues. *Space Sci. Rev.* **141,** 477–508 (2008).
31. Bonnell, J. W. *et al.* The electric field instrument (EFI) for THEMIS. *Space Sci. Rev.* **141,** 303–341 (2008).

32. Le Contel, O. *et al.* First results of the THEMIS search coil magnetometers. *Space Sci. Rev.* **141,** 509–534 (2008).
33. El-Alaoui, M. *et al.* Substorm evolution as revealed by THEMIS satellites and a global MHD simulation. *J. Geophys. Res.* **114,** A08221 (2009).
34. Ashour-Abdalla, M., El-Alaoui, M., Coroniti, F. V., Walker, R. J. & Peroomian, V. A new convection state at substorm onset: Results from an MHD study. *Geophys. Res. Lett.* **20,** 1965 (2002).
35. Ashour-Abdalla, M., Berchem, J. P., Büchner, J. & Zelenyi, L. M. Shaping of the magnetotail from the mantle—Global and local structuring. *J. Geophys. Res.* **98,** 5651–5676 (1993).
36. Schriver, D., Ashour-Abdalla, M. & Richard, R. L. On the origin of the ion-electron temperature difference in the plasma sheet. *J. Geophys. Res.* **103,** 14879–14896 (1998).
37. Schriver, D. *et al.* in *Proceedings of the 7th ISSS* 345–346 (Research Institute for Sustainable Humanosphere (RISH), Kyoto University, 2005).
38. Büchner, J. & Zelenyi, L. M. Chaotization of the electron motion as the cause of an internal magnetotail instability and substorm onset. *J. Geophys. Res.* **92,** 13456–13466 (1987).
39. Büchner, J. & Zelenyi, L. M. Regular and chaotic charged particle motion in magnetotaillike field reversals. I—Basic theory of trapped motion. *J. Geophys. Res.* **94,** 11821–11842 (1989).

Acknowledgements

We thank H. Kohne for help with programming and display of the data and simulation results. Research at UCLA was supported by NASA grant NNX08AO48G. We acknowledge NASA contract NAS5-02099 and V. Angelopoulos for use of data from the THEMIS Mission, specifically, C. W. Carlson and J. P. McFadden for the use of ESA data, D. Larson and R. P. Lin for the use of SST data, K. H. Glassmeier, U. Auster and W. Baumjohann for the use of FGM data, J. W. Bonnell and F. S. Mozer for the use of EFI data, and A. Roux and O. LeContel for the use of SCM data. K-J.H. and M.L.G. were supported, in part, by NASA's Magnetospheric Multiscale and Cluster missions at the Goddard Space Flight Center. M.G.K. was supported, in part, by NASA Grant UCB NAS 5-02099. The computing was carried out on NASA's Columbia Supercomputer.

Author contributions

M.A-A. initiated the electron acceleration study using observations and simulations. She led the research project, participated in the analysis of all of the simulation and observation results. M.E-A. carried out the MHD simulations and identified the dipolarization fronts in the Global model. He also participated in the analysis. M.G. was the first to realize the importance of this study. From his experience of Cluster data, he realized the wide applicability of these results. M.Z. carried out the particle simulations and participated in the analysis of the particle results. D.S. participated in the analysis of the particle results. R.R. developed the algorithm for converting simulation counting rates into differential energy flux and carried out the betatron acceleration analysis. R.W. participated in the analysis of the simulation results with emphasis on the MHD results. M.G.K. helped with theoretical issues; in particular she suggested analysis to quantify the betatron acceleration. K-J.H. applied experience she gained from studying electron acceleration during other dipolarization events seen by Cluster.

Additional information

The authors declare no competing financial interests. Supplementary information accompanies this paper on www.nature.com/naturephysics. Reprints and permissions information is available online at http://npg.nature.com/reprintsandpermissions. Correspondence and requests for materials should be addressed to M.A-A.